www.aem-iournal.com

Toward Control of Microstructure in Microscale Additive Manufacturing of Copper Using Localized Electrodeposition

Soheil Daryadel, Ali Behroozfar, and Majid Minary-Jolandan*

The progress in microscale additive manufacturing (μ-AM) of metals requires engineering of the microstructure for various functional applications. In particular, achieving in situ control over the microstructure during 3D printing is critical to eliminate the need for post-processing and annealing. Recent reports have demonstrated the possibility of electrochemical μ-AM of nanotwinned metals, in which the presence of parallel arrays of twin boundaries (TBs) are known to enhance mechanical and electrical properties. For the first time, the authors report that the microstructure of metals printed using the microscale localized pulsed electrodeposition (L-PED) process can be controlled in situ during 3D-printing. In particular, the authors show that through electrochemical process parameters the density and the orientation of the TBs, as well as the grain size can be controlled. The results of the in situ SEM microcompression experiments on directly 3D-printed micro-pillars show that such control over microstructure directly correlates with the mechanical properties of the printed metal.

1. Introduction

The control of microstructure in 3D-printed metals is one of the most formidable challenges facing microscale additive manufacturing (μ -AM) of these materials. The main focus of μ -AM processes for metals has been on achieving small scale structures with complex geometries. However, for functional applications (such as electronics, sensors, photonic, among others) with desirable properties, it is necessary to gain control over of the microstructure, and hence mechanical and electrical properties. The mechanical properties (such as yield stress, flow stress and strength) of metals and alloys are predominantly determined by their microstructure including the grain size, dislocation density, and dislocation mobility, and the solid solution content. Electrical properties are often affected by

Dr. M. Minary-Jolandan Alan G. MacDiarmid NanoTech Institute The University of Texas at Dallas Richardson, TX 75080, USA E-mail: majid.minary@utdallas.edu

Dr. S. Daryadel, Dr. A. Behroozfar, Dr. M.Minary-Jolandan Department of Mechanical Engineering The University of Texas at Dallas Richardson, TX 75080, USA

DOI: 10.1002/adem.201800946

impurities and defects in the material. Currently, there is very limited information on the control of microstructure in μ -AM of metals.

Several distinct physical and chemical μ-AM processes for metals are currently available. They include direct ink writing electrohydrodynamic printing (DIW), (EHD), local electrophoretic deposition, laser-induced forward transfer (LIFT), meniscus-confined electroplating, electroplating of locally dispensed ions in liquid, laserinduced photoreduction, and traditional focused electron/ion beam induced deposition processes.^[1] DIW and EHD often require post-processing to remove the organic matrix from the printed composite. Heat treatment, often as high as 400-500°C decomposes the polymer matrix, and results in densification and grain growth of the metallic phase. Pronounced porosity can also result from the heat

treatment. Removal of the polymer matrix may enhance the electrical conductivity of the material, however, the grain growth during annealing is not desirable for mechanical properties. The microstructure in LIFT and reduction-based approaches is often crystalline, and the microstructure can be potentially controlled through process parameters in situ.

The localized pulsed electrodeposition (L-PED) is an electrochemical-based microscale additive manufacturing process (μ-AM) for metals and alloys.^[3] In this process, electrodeposition is confined to a small zone at the tip of a nozzle filled with the liquid electrolyte of the metal of interest (Figure 1a). When the nozzle approaches to the substrate, a meniscus (liquid bridge) is formed between the tip of the nozzle and the conductive substrate. This electrolyte meniscus functions as a confined electrochemical bath (Figure 1b). When a pulsed electric potential is applied (Figure 1d) between an electrode inserted from the back of the nozzle (the counter electrode, or anode) and the substrate (the working electrode, or cathode), the metal ions are deposited at the growth front within the meniscus area on the cathode surface.^[4] The localized electrodeposition can be used for 3D printing of any metallic material that can be electrodeposited, including alloys. However, so far deposition of limited number of metals including copper, platinum, and gold has been reported, and the remaining materials remain as future work.

In the L-PED process, the applied potential/current is interchanged repeatedly between ON and OFF with the time

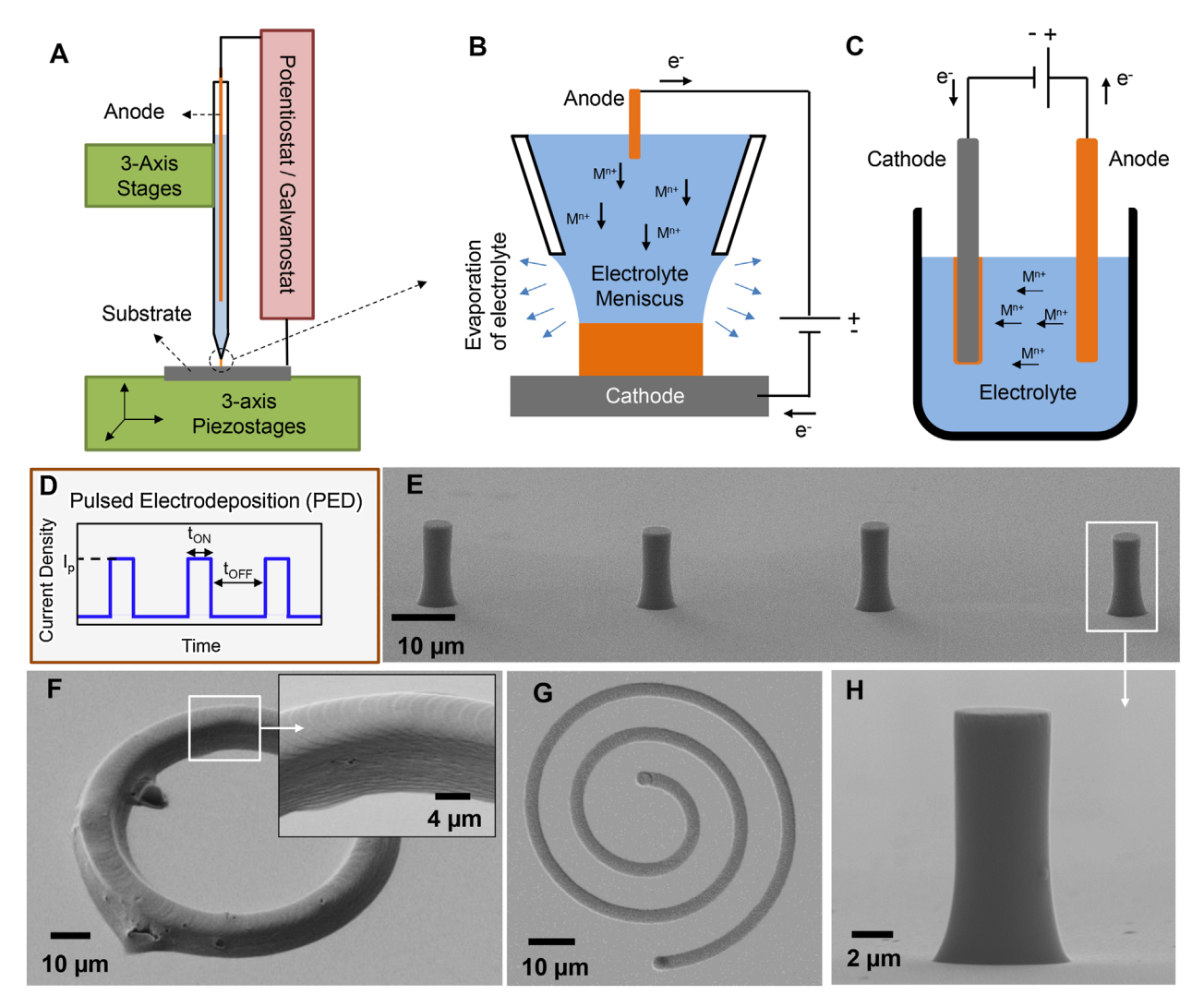


Figure 1. a) The schematic view of L-PED 3D printing process. Side-by-side comparison of (b) the L-PED printing process and (c) the bulk electrodeposition. d) Pulsed current electrodeposition (PED) with an arbitrary duty cycle. SEM images of (e) an array of 3D-printed μ-pillars for microcompression experiment (printing time for each pillar \approx 12 min), f) a 40-Layer structure printed by layer-by-layer L-PED (printing time \approx 150 min), g) a spiral pattern (printing time \approx 15 min), and h) a close-up view of a μ-pillar for micro-compression and microstructure characterization.

periods of $T_{\rm ON}$ and $T_{\rm OFF}$, respectively (Figure 1d). Therefore, during short time interval of ON potential, a very high current density and subsequently high deposition rate is achieved, while in the OFF-time the consumed ions are recovered, and higher concentration of ions is provided on the cathode surface for the subsequent ON-time. In pulsed electrodeposition (PED) the ON-time is often on the order of milliseconds, and the OFF-time is on the order of seconds. High purity metallic structures can be printed in desired 3D geometries through precise and controlled motion of the relative position of the nozzle and the substrate. L-PED is capable of printing different geometries such as free-standing wires, micro-pillars (μ -pillars), and layer-by-layer structures (Figure 1e–h).

The L-PED process can be used to produce unique microstructures that are not obtainable by conventional direct current electrodeposition (DC-ED). The meniscus-confined DC electrodeposition was demonstrated in 2010 for 3D printing of microscale copper (Cu) wire bonds.^[2a] The metal printed by DC-ED is nanocrystalline.^[5] Recently, we reported that by application of pulsed current/voltage, high purity and void-free nanotwinned Cu can 3D-printed without any additives.^[3] Nanotwinned metals are ultrafine-grained or fine-grained metals with grains that contain a high density of layered nanoscale twins divided by coherent twin boundaries (TBs). Nanotwinned metals have an unprecedented combination of ultrahigh strength, high ductility, and high electrical conductivity,^[6] and are hence attractive for applications requiring high electrical conductivity and high strength and ductility such as in flexible electronics, sensors, solder bumps, interconnects, and wire bonds.

Although pulsed electrodeposition at bulk scale has been previously studied, however, bulk PED and L-PED have several major differences. These differences are discussed in the SI. Considering these differences between the bulk PED and L-PED, kinetics of electrodeposition, flow of electrolyte, concentration of

www.advancedsciencenews.com

www.aem-iournal.com

ADVANCED ENGINEERING MATERIALS

ions, distribution of electric potential, and the current density, which ultimately determine the average deposition rate may be different between the electrodeposition in a confined nozzle versus conventional electrodeposition in a bath. Hence, we aim to investigate the effect of various process parameters on the microstructure and mechanical properties of the 3D printed metal using L-PED.

2. Results and Discussion

For this study, several tens of copper (Cu) micro-pillars (μ -pillars) with a diameter of $\approx 5~\mu m$ were directly 3D-printed using the L-PED process with different processing parameters. Similar μ -pillars are often fabricated using the focused ion beam (FIB) milling from thin films of the material of interest. The L-PED process enables direct printing of the μ -pillars, which facilitates characterization of both microstructural and mechanical properties. Details of the printing process is given in the materials and method section. Figure 1e shows a SEM image of an array of four μ -pillars with diameter of $\approx 5.2~\mu m$ printed for the in situ SEM micro-compression experiment. The μ -pillars have uniform geometry throughout the length with a strong adhesion to the substrate, which is important for quantitative characterization of mechanical properties.

The energy dispersive X-ray spectroscopy (EDS) spectra acquired from a μ -pillar (Figure 1h) is shown in **Figure 2**a. The EDS data show that the printed material is high purity Cu without significant presence of impurities (Figure S1). Although

the printing process is carried out in room environment, only small amount of oxygen is present on the surface of the substrate and μ -pillars. Note that the gold (Au), chromium (Cr), and silicon (Si) in the spectra originated from the substrate.

Three independent variables in PED include $T_{\rm ON}$, $T_{\rm OFF}$, and the peak current density (I_P), as shown in Figure 1d. The average current density (I_A) in PED is defined as $I_A = I_P \times \gamma$, in which γ is the duty cycle, $\gamma = T_{\rm ON}/(T_{\rm ON} + T_{\rm OFF})$. Often time, the average current density is used as the main process parameter in PED. Increasing the average current density results in increase in the deposition rate. For growth of a μ -pillar, it can be shown that the growth rate (which is equal to the withdrawal speed of the nozzle) is given by $\frac{4iM}{nF\rho\pi D^2}$ in which i is the applied current during deposition, M is the molar mass and ρ is the mass density of the deposited material, n is the number of electrons per ion involved in the deposition reaction, F is the Faraday constant, and D is the diameter of the μ -pillar. $I^{(2a)}$ This relationship shows that the deposition rate is proportional to the average current density $I^{(4i)}$.

Figure 2b shows the experimental deposition rate for the printed μ -pillars by the L-PED process versus the average current density. The data shows a linear trend between the deposition rate and the average current density. The solid line is the deposition rate calculated form the Faraday's law. The current efficiency (CE) of the L-PED process can be calculated as the ratio of the experimental deposition rate and the deposition rate calculated from the Faraday's law.^[7] The obtained current efficiency of the L-PED process was calculated to be $90\pm5\%$,

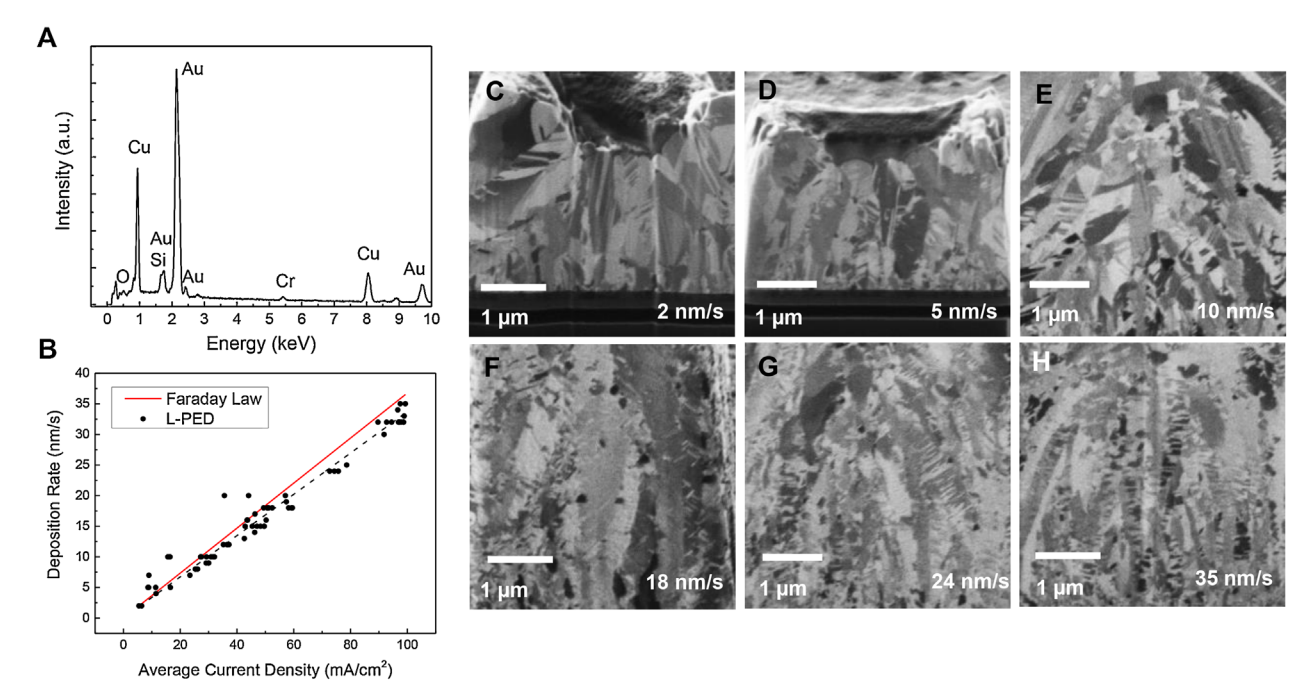


Figure 2. a) The EDS spectra acquired from a printed μ -pillar. No significant presence of impurities was observed in EDS data. b) The experimental deposition rate for the printed μ -pillars by the L-PED process versus the average current density. The solid line is the deposition rate calculated from the Faraday's law. The current efficiency of the L-PED process was calculated to be 90 ± 5%. c–h) The effect of the average current density (and deposition rate) on the microstructure of 3D-printed nanotwinned Cu μ -pillars. The cross-section FIB ion channeling contrast image of μ -pillars printed at different deposition rates reveal that increasing the deposition rate increases the density and alignment of the twin boundaries (TBs).

ADVANCED ENGINEERING MATERIALS

which implies minimum side reactions and "wasted" current in the process. The high CE also implies that the side reactions do not produce any significant impurities in the deposited metal, as also confirmed by the EDS data (Figure 2a, S1).

The density of twins that are formed during the deposition process highly depends on the nucleation rate and the average deposition rate. $^{[6b]}$ In the bulk PED, it has been shown that the systematic change of the average current density enables synthesizing nanotwinned Cu with different twin thickness. $^{[6b]}$ We examined the effect of average current density (hence the deposition rate) on the microstructure of the printed metal by the L-PED process. Detailed deposition parameters for the $\mu\text{-pillars}$ are presented in Table S1.

Figure 2c–h show the cross-section FIB ion channeling contrast images of six different $\mu\text{-pillars}$ deposited at different average current densities, spanning from $\approx\!5$ to $\approx\!100\,\text{mA}\,\text{cm}^{-2}.$ This range of average current density results in deposition rates spanning 2 to 35 nm s $^{-1}.$ The results show that for this range of parameters, all the printed Cu $\mu\text{-pillars}$ contain twin boundaries (TBs). By increasing the average current density and the average deposition rate, the density of the TBs increases, which results in refinement of the twin lamella thicknesses. Additionally, we observed that for slower deposition rate, TBs are randomly ordinated within the grains. As the deposition rate increases, the grains become more columnar and the TBs within the grains get more aligned perpendicular to the growth direction.

The average current density and accordingly the deposition rate in PED process can be engineered by adjusting different pulse parameters including the peak current density, ON-time, and OFF-time. We investigated the influence of each of the pulse parameters on the microstructure of the printed Cu (Figure 3). In electrodeposition process, after transfer and incorporation of the ions on the cathode surface, there are two competitive processes depending on the electrochemical parameters: building up of the existing crystals or growing new ones.[8] The increase in the peak current density favors the nucleation of new crystals rather than the building up the existing ones. μ-pillars were deposited using pulsed currents with the same periodic $T_{\rm ON}/T_{\rm OFF}$ ratio (20 ms 2 s⁻¹) and different peak current densities. As can be observed in Figure 3a and b, increasing the peak current density from 2.77 to 9.85 A cm⁻² (corresponding to the deposition rate of $10 \,\mathrm{nm \, s^{-1}}$ and $35 \,\mathrm{nm \, s^{-1}}$, respectively) increased the twin density in the metal, and also decreased the grain size. The metal printed with smaller average current density exhibits randomly-shaped large grains with few randomly-oriented TBs, while the metal printed with the higher peak current density shows smaller columnar-shaped grains with high density of aligned TBs.

The duty cycle is an important parameter in the L-PED process, which is a function of $T_{\rm ON}$ and $T_{\rm OFF}$. In order to investigate the effect of the ON-time on the microstructure of the 3D-printed Cu, μ -pillars were fabricated using approximately the same peak current density and OFF-time, with different ON-time. The

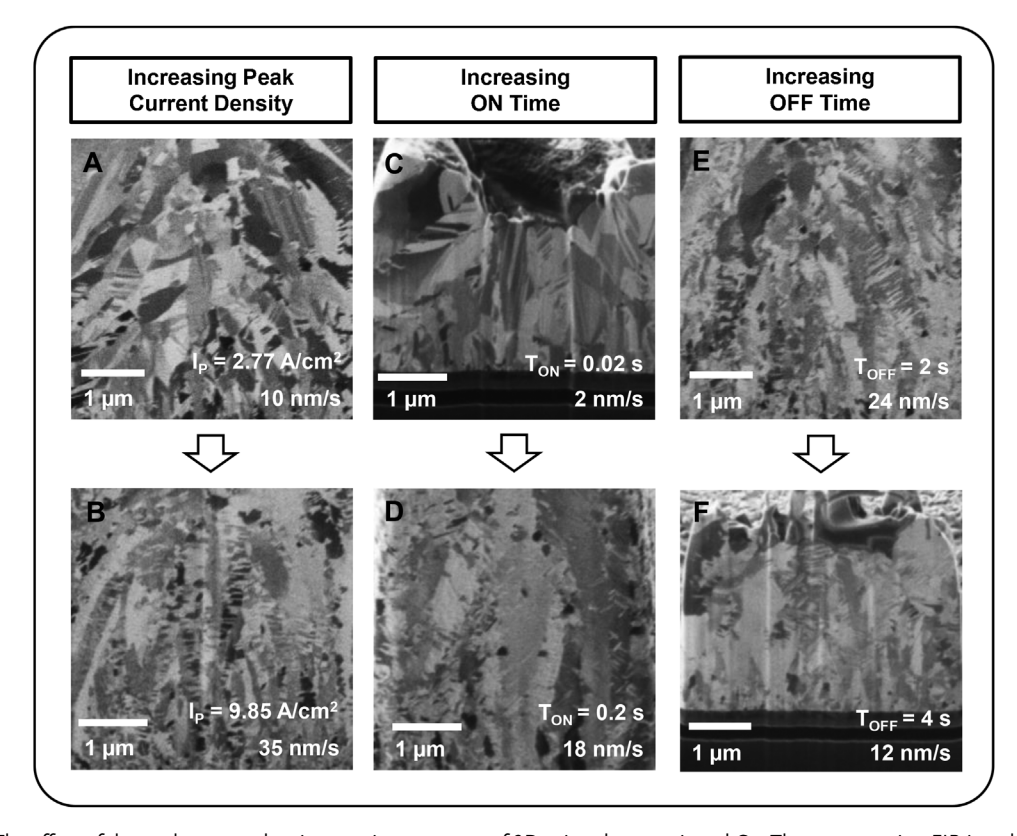


Figure 3. a), b) The effect of the peak current density on microstructure of 3D-printed nanotwinned Cu: The cross-section FIB ion channeling contrast image show that increasing the peak current density increased the twin density and decreased the grain size. c), d) increasing the ON-time results in higher density of twin boundaries. e), f) increasing the OFF-time decreases the twin density and increases the grain size.

ADVANCED ENGINEERING MATERIALS

deposition peak current density was kept at \approx 0.6 A cm⁻² and $T_{\rm OFF}$ was set to 2 s, while the $T_{\rm ON}$ was increased from 20 to 200 ms. Increase of the ON-time results in higher density of TBs as can be observed in Figure 3c and d. This increase in the number of TBs is because of the increase in the average current density by nearly ten times (\approx 5.5 to \approx 59.2 mA cm⁻²). Although there is no significant grain refinement, however, the grains are more aligned with columnar shape. The columnar-shaped grains often tend to grow along the fast growth direction of the metal. ^[9]

One of the most important parameters in PED is the time interval between two pulses, or the OFF-time. Although no current is applied during the OFF-time, it is believed that this period is very active with respect to recrystallization of the deposited metal. It is believed that the TBs are formed during the growth interruption and stress relaxation during the OFF-time. [10] Figure 3e and f show two different $\mu\text{-pillars}$ printed using approximately the same peak current density and ON-time, and different OFF-time duration. Increasing the OFF-time from 2 to 4 s, decreased the average deposition rate from 24 to $12\,\mathrm{nm\,s^{-1}}$, and the average current density from ≈ 72.7 to $\approx 34.7\,\mathrm{mA\,cm^{-2}}$. As a result, the density of the TBs in the printed metal decreased.

Additionally, the metal deposited using a longer $T_{\rm OFF}$ has significantly larger grains compared to the metal printed using shorter $T_{\rm OFF}$. In the L-PED process, the current interruption causes desorption of impurities and inhibitors from the deposits and replenishment of the metal ions in the diffusion layer. [11]

This phenomenon may produce opposite outcomes in terms of crystallization mechanism for different metals. For Cu deposition, increase in the OFF-time stimulates grain growth rather that forming new grains, because in this system, the larger grains are thermodynamically more stable, and the system reaches the most stable state for longer $T_{\rm OFF}$. [8,11] As can be observed in the cross-section of the pillar in Figure 3f, increasing the $T_{\rm OFF}$ increased the grain size of the metal. When $T_{\rm OFF}=0$, the process is essentially DC-ED. The effect of the processing parameters on the microstructure of the printed metal using DC-ED process is discussed in the SI.

The mechanical properties of selected nanotwinned Cuu-pillars were characterized using in situ SEM microcompression experiments in order to investigate the microstructure-property relationship of the printed copper by the L-PED process. We examined the mechanical properties of the µ-pillars printed at three different deposition rates of 10, 18, and 24 nm s⁻¹ corresponding to average current densities of ≈ 27.5 , ≈ 59.2 , and \approx 72.7 mA cm⁻², respectively. Figure 4a shows an SEM image of the microcompression experiment on an array of printed Cu μpillars. It is noteworthy that the geometry of the nozzle limits the minimum achievable spacing between two micro-pillars. However, using appropriate pulling parameters, nozzles can be fabricated with long taper to avoid touching the pipette with previously printed pillar. A zoomed-in view of one the μ -pillars after the compression experiment is shown in Figure 4b. A movie of the compression experiment is provided as a supporting document.

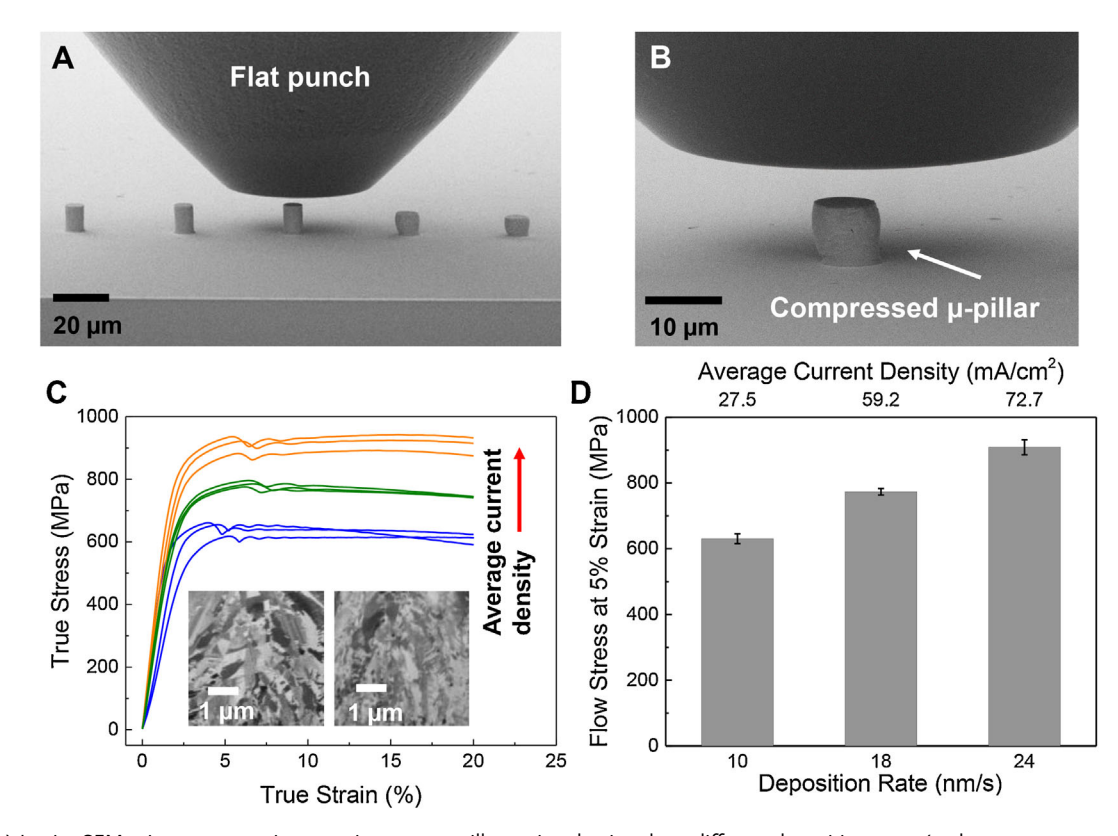


Figure 4. a) In situ SEM micro-compression experiment on μ -pillars printed using three different deposition rates (and average current densities). b) SEM image of a compressed μ -pillar. c) Stress versus strain responses of the μ -pillars printed in three different deposition rates. d) Comparison of the average flow stress of each microstructure.

ADVANCED ENGINEERING MATERIALS

The compression stress–strain responses of the μ-pillars are presented in Figure 4c. The true stress-strain was obtained by assuming a constant volume for the material during compression. Figure 4d is the comparison of the flow stress for the printed metal at different deposition rates and average current densities. Several observation can be made. First, variations in the stress-strain responses for the u-pillars printed with the same parameters are low. This indicates that the process is repeatable and the obtained microstructure is consistent. Second, a near-perfect elasto-plastic behavior with a smooth flow stress and no noticeable hardening is observed in compression stress-strain responses. There is a slight drop in the flow stress in the transition to the plastic region after the peak stress, which is attributed to the sudden initiation of the plastic deformation after dislocations pile-up against the TBs up to the point of maximum stress.^[12] In nanotwinned Cu, the TBs effectively block the motion of dislocations similar to the grain boundaries, while they create more local sites for nucleation of dislocations. They also accommodate dislocation motion to elevate the ductility of the material.

Third, there is a clear difference between stress–strain responses of the $\mu\text{-pillars}$ printed with different average current densities. The flow stress of the $\mu\text{-pillars}$ deposited at $10~\text{nm s}^{-1}$ ranged from 616 to 646 MPa with an average of 630 ± 15 MPa. The flow stress of the $\mu\text{-pillars}$ deposited at 18 nm/s ranged from 765 to 784 MPa with an average of 773 ± 9 MPa. And the flow stress of the $\mu\text{-pillars}$ deposited at 24 nm/s ranged from 885 to 931 MPa with an average of 909 ± 23 MPa. As shown in Figure 2, increasing the deposition rate in the L-PED process results in formation of grains with more aligned TBs and higher density of TBs. Densely packed printed nanotwinned Cu using the deposition rate of $24~\text{nm s}^{-1}$ and the average current density

of \approx 72.7 mA cm⁻² exhibited \approx 44% higher flow stress compared to the Cu printed at the deposition rate of 10 nm s⁻¹ and the average current density of \approx 27.5 mA cm⁻². Lastly, overall the strength of the printed metal is remarkable, considering that often time mechanical properties of the printed materials are inferior compared to their counterparts fabricated with other processing methods. A yield strength in the range of 600 to over 900 MPa is several times of the bulk Cu. We note that the diameter of the μ -pillars is large enough so that there is no size-effect in the obtained properties.

It is believed that dislocations originated at the grain boundary triple junctions due to the stress concentration. [12] In the nanotwinned metal the partial dislocations are not only blocked by the grain boundaries, but also TBs similarly block the intersecting slip planes. Dislocations are only allowed to propagate parallel to the TBs, and they pile up at the boundaries. The strength of the specimen increases by higher density of TBs following the Hall-Petch relation.[6b] Additionally, for a metal with columnar-shaped grains, the plane orientation of the TBs with respect to the load direction significantly affects the strength. [9] The highest compression yield strength and flow stress are achieved when the loading axis is perpendicular to the planes of the TBs. [13] Therefore, the mechanical behavior of such materials strongly depend on the density and orientation of TBs. Well-aligned and high density of TBs result in a lower density of stacking faults in the columnar grains, which enhances the strength of the metal.[12]

Figure 5 shows a summary of the process-microstructure-property relationships for microscale printed Cu using the L-PED process. Employing constant current density in DC-ED mode results in nanocrystalline microstructure. Increase in the applied current density in DC-ED mode decreases the size of the

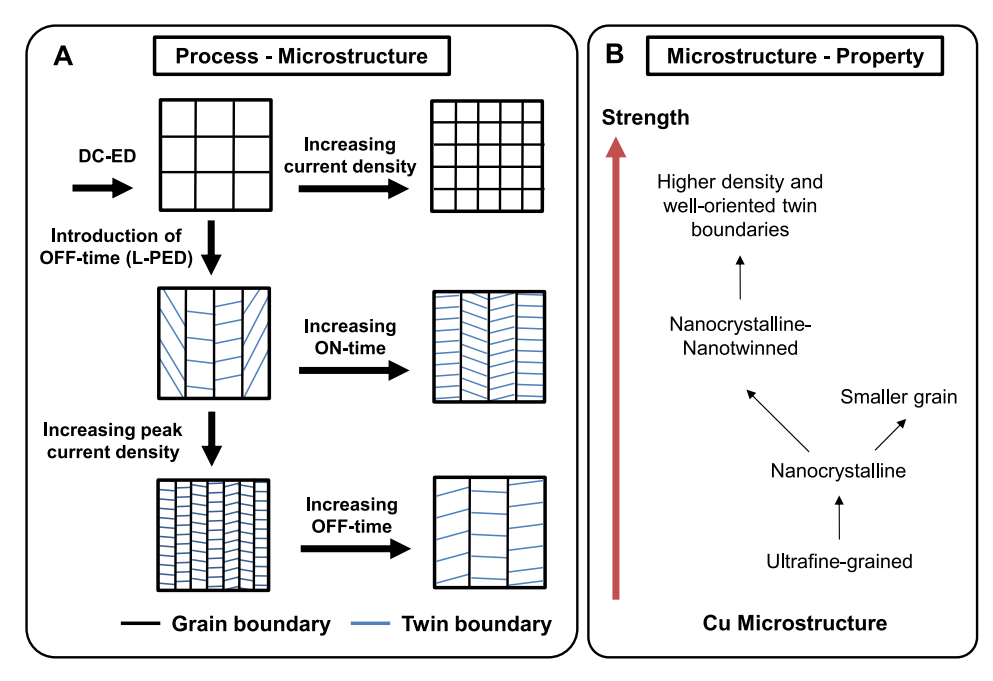


Figure 5. Illustration of a) process – microstructure and b) microstructure – property relations in microscale 3D printing of Cu by localized pulsed electrodeposition (L-PED) process.



www.advancedsciencenews.com

www.aem-iournal.com

ADVANCED ENGINEERING MATERIALS

grains through increase in the nucleation rates. The effect of process parameters in DC-ED mode is presented in the SI. Interestingly, PED by introduction of the OFF-potential during the process enables printing of nanotwined Cu. Results revealed that deposition parameters in PED have significant effect on the microstructure of the printed metal. Raising the ON-time increases the density of TBs and their alignment within the grains by increasing the average current density and deposition rate. Boosting up the peak current density increases the twin density while decreasing the grain size significantly. Moreover, increasing the OFF-time period increases the grain size while decreasing the twin density.

Nanocrystalline Cu is known to be stronger than ultrafine-grained Cu because more grain boundaries can block the partial dislocations within the material. Therefore, based on the Hall–Petch relation, [14] decreasing the grain size results in an increase in the strength of the metal. The introduction of TBs within the grains increases the strength, since TBs can block the intersecting slip planes similar to the GBs. [15] Hence, the strength increases with increasing twin density, following the Hall–Petch relation. [6b] Additionally, the orientation of the TBs has significant effect on the strength of nanotwinned Cu; more aligned TBs results in a much lower density of stacking faults within the grains and enhances the strength. [12]

3. Conclusions

The promise of microscale additive manufacturing (μ-AM) of metals is that the material is added layer by layer to form a desired geometry for various functional applications such as electronics, sensors, photonic, among others. Since the microstructure of a metal governs its mechanical and electrical properties, in addition to the geometry the microstructure of the metal needs to be also engineered to achieve desired material properties. Our experimental results show that in the localized pulsed electrodeposition (L-PED) µ-AM process, the average current density is the critical electrochemical process parameter for the control of the microstructure of the 3D printed copper. Increase in the average current density enhances the deposition rate of the metal, and in turn, results in the increase in the density of the twin boundaries (TBs), increase in the alignment of the TBs within the grains, and transition to columnar grains from randomly oriented grains. The results of the in situ SEM nanomechanical experiments show that such change in the microstructure directly enhances mechanical properties of the 3D-printed metal. Specifically, \approx 1.7-fold increase in the average current density results in \approx 1.4-fold increase in the deposition rate of the metal, which results in ≈44% enhancement in the flow stress of the printed metal. Specifically, the results show that the flow stress of the 3D-printed nanotwinned copper can be tuned from \approx 630 to \approx 910 MPa (3–5 times of the bulk copper) by changing the microstructure during the printing.

4. Experimental Section

For printing Cu μ-pillars glass micropipettes were pulled to desired diameters using a pipette puller (Model P-97, Sutter Instrument). Each

nozzle was filled with the electrolyte solution of $CuSO_4$ (100 mM) and H_2SO_4 (1 M). Additionally, the cell consists of a conductive substrate (gold-coated silicon) as the working electrode, and a copper wire inserted from back of the nozzle as the counter electrode. A potentiostat/galvanostat (VersaSTAT 4, Princeton Applied Research) was utilized to control the electric potential between the two electrodes and provide real-time feedback during the electrodeposition process. A fine resolution (4 nm) three-axis nano-positioning linear stage was employed to control the position and velocity of the substrate during printing. During the process, the humidity around the nozzle was controlled by a remote hygrometer, and 3D printing was conducted at a constant relative humidity of $\approx\!60\%$. The printing procedure was observed in situ using a high-resolution monitoring system consisting of a long working distance optical objective lens coupled with a CCD camera (XM-10, Olympus).

It is noteworthy that there are differences in the chosen range of parameters in the L-PED process compared to the bulk PED. For instance, while there is no lower limit in the deposition rate in PED, due to the essential fact that in L-PED process the deposition rate should be synced with the steady speed of the nozzle. [3a] Therefore, parameters should be chosen in a way that the slowest deposition rate meets the lower limit speed of the positioning stages. This limit in our experiment was $1\,\mathrm{m\,s^{-1}}$. Additionally, there is an upper limit for the applied peak current density to avoid clogging of the nozzle due to fast and dendritic deposition of material.

The microstructure of the 3D-printed micro-pillars were characterized using scanning electron microscopy (SEM), energy dispersive X-ray spectroscopy (EDS), and high-resolution focused ion beam (FIB). The overall geometry, diameter, and height of the micro-pillars were observed under SEM (Zeiss Supra 40) to examine if they were suitable for microcompression experiment. Elemental analysis was performed using the same system equipped with an EDS system using 18 kV electron beam. To examine the grain size and twin boundary presence, the cross-section of the micro-pillars was observed using high-resolution focused ion beam (FIB) imaging (FEI Nova Nanolab 200). The cross-section of the micro-pillars was milled at a final acceleration voltage of 30 keV and current of 10 pA, followed by imaging using the same parameters.

Mechanical properties of the 3D-printed μ-pillars were obtained using microcompression experiments in situ SEM by a nanoindentation system (NanoFlip, Nanomechanics). Micro-pillars were compressed using a 50 μm diameter flat punch conductive diamond as the compression anvil. Three samples were tested for each deposition parameter that was examined for mechanical properties. The diameter range of the micropillars was $\approx 5.10 \pm 0.7 \,\mu m$. To minimize the effects of buckling and the other artifacts, the length-to-diameter aspect ratio of the μ -pillars was kept at \approx 2:1. For accurate microcompression experiment, the top surface of the micro-pillars were milled with FIB to completely flatten their top surface, where the tip of the flat punch touches the printed metal. Fine milling was performed at an acceleration voltage of 30 keV and current of 10 pA. All experiments were run under displacement-control mode at a constant displacement rate in order to achieve the constant strain rate of $1 \times 10^{-3} \, \mathrm{s^{-1}} \, (\dot{\epsilon} = \dot{\ell} / 1)$. The stress–strain response was calculated based on the obtained load-displacement and geometry of each micro-pillar. Real-time deformation video and the mechanical data were recorded during the experiments.

Acknowledgement

This work was supported by the NSF-CMMI (award # 1727539) and US Office of Naval Research (award # N00014-15-1-2795).

Conflict of Interest

There are no conflicts to declare.



www.advancedsciencenews.com

www.aem-iournal.com

ADVANCED ENGINEERING MATERIALS

Supporting Information

Supporting Information is available from the Wiley Online Library or from the author.

Keywords

localized electrodeposition (LED), micro-scale additive manufacturing (μ -AM) of metals, microstructural control, nanotwinned metals

Received: September 1, 2018 Revised: October 15, 2018 Published online:

- L. Hirt, A. Reiser, R. Spolenak, T. Zambelli, Adv. Mater. 2017, 29, 1604211.
- [2] a) J. Hu, M.-F. Yu, Science 2010, 329, 313; b) H. Luca, I. Stephan,
 P. Zhijian, D.-C. Livie, R. Alain, J. M. Wheeler, F S. S Ralph, V. János,
 Z. Tomaso, Adv. Mater. 2016, 28, 2311; c) B. Y. Ahn, E. B. Duoss,
 M. J. Motala, X. Guo, S.-I. Park, Y. Xiong, J. Yoon, R. G. Nuzzo,
 J. A. Rogers, J. A. PN Lewis, Science 2009, 323, 1590.
- [3] a) S. Daryadel, A. Behroozfar, S. R. Morsali, S. Moreno, M. Baniasadi,
 J. Bykova, R. A. Bernal, M. Minary-Jolandan, *Nano Lett.* 2018, 18,
 208; b) A. Behroozfar, S. Daryadel, S. R. Morsali, S. Moreno,

- M. Baniasadi, A. Bernal Rodrigo, M. Minary-Jolandan, Adv. Mater. 2017, 30, 1705107.
- [4] a) S. Morsali, S. Daryadel, Z. Zhou, A. Behroozfar, M. Baniasadi, S. Moreno, D. Qian, M. Minary-Jolandan, J. Appl. Phys. 2017, 121, 214305; b) S. Morsali, S. Daryadel, Z. Zhou, A. Behroozfar, D. Qian, M. Minary-Jolandan, J. Appl. Phys. 2017, 121, 024903.
- [5] A. P. Suryavanshi, M.-F. Yu, Appl. Phys. Lett. 2006, 88, 083103.
- [6] a) L. Lu, Y. Shen, X. Chen, L. Qian, K. Lu, Science 2004, 304, 422; b)
 L. Lu, X. Chen, X. Huang, K. Lu, Science 2009, 323, 607.
- [7] A. J. Bard, L. R. Faulkner, W. John, Sons, Electrochemical Methods: Fundamentals and Applications, John Wiley & Sons, Hoboken 2007.
- [8] J. C. Puippe, F. Leaman, E. American, U. h. b. g. c. b. i. j. Surface Finishers Society, *Theory and Practice of Pulse Plating*, American Electroplaters and Surface Finishers Society, 1986. ISBN-10: 0936569026, ISBN-13: 978-0936569024.
- [9] I. A. Ovid'ko, A. G. Sheinerman, Rev. Adv. Mater. Sci. 2016, 44, 1.
- [10] D. Xu, W. L. Kwan, K. Chen, X. Zhang, V. Ozolinš, K. N. Tu, Appl. Phys. Lett. 2007, 91, 254105.
- [11] T. Pearson, K. Dennis, Trans. Inst. Met. Finish. 1991, 69, 75.
- [12] Z. X. Wu, Y. W. Zhang, M. H. Jhon, J. R. Greer, D. J. Srolovitz, Acta Mater. 2013, 61, 1831.
- [13] M. Mieszala, G. Guillonneau, M. Hasegawa, R. Raghavan, J. M. Wheeler, S. Mischler, J. Michler, L. Philippe, *Nanoscale* 2016, 8, 15999.
- [14] a) N. J. Petch, J. Iron Steel Inst. 1953, 173, 25; b) E. O. Hall, Proc. Phys. Soc. Sect. B 1951, 64, 742.
- [15] D. Jang, X. Li, H. Gao, J. R. Greer, Nat. Nanotechnol. 2012, 7, 594.

Supplementary Information

Toward Control of Microstructure in Microscale Additive Manufacturing of Copper Using Localized Electrodeposition

Soheil Daryadel¹, Ali Behroozfar¹, and Majid Minary-Jolandan^{1,2}

¹Department of Mechanical Engineering, ²Alan G. MacDiarmid NanoTech Institute, The University of Texas at Dallas, Richardson, TX 75080, US

*Corresponding Author E-mail: majid.minary@utdallas.edu

In principle, it is possible to achieve more complex 3D geometries including hollow cylinders, overhang wires, and helical geometry etc. by modifying the process parameters and by modifying the nozzle tip to enable accurate printing at low angle and lateral motion. Based-on the complexity of a 3D model, certain 3D prints require support structures. The models printed in this study using L-PED did not need any support structures, however for more complex model L-PED can address this concern with additional nozzle/channel for print of support structure if required. Additionally, in the L-PED process the size of the patterns are only limited by the travel range of the printing stages. In this study, our fine motion printing stage has the range of 80 µm.

Bulk PED has been extensively investigated in the literature.^[2] Generally, it is known that the microstructure of the deposited metal is dependent on the deposition parameters and conditions, such as stirring, bath additives, temperature, and the pH.^[3] PED facilitates more control over the microstructure compared to the conventional DC method because of the inclusion of ON-and OFF-time. The mechanisms for control of the grain texture and twin densities are reported in the literature by changing the peak current density and duty cycle.^[2b-e] However, L-PED is inherently distinct from the bulk PED. Figure 1B and C show the side-by-side comparison of the L-PED with the conventional bulk electrodeposition. In conventional (pulsed) electrodeposition,

the anode and cathode are immersed into an electrolyte bath. Hence, the entire cathode surface is exposed to the electrolyte and pulsed current. In L-PED only the area under the meniscus (liquid bridge) is exposed to the electrolyte. Considering the small size of the cathode area (radius of smaller than 25 µm) in this process, we can assume the electrode in the system as an ultramicroelectrode (UME). In UMEs, as the dimension of the electrode is comparable to the thickness of the double layer. The small size of the cathode electrode generates small overall passing currents, and consequently a very low ohmic drop, which allows using simple two-electrode cell instead of the conventional three-electrode.

The short pulses applied to the anode by the potentiostat during *Ton* drives the ions and hence the electrolyte toward the cathode, which generates a convective flow in the narrow nozzletip and within the meniscus. [5] High concentration of metal ions in the meniscus area during *Ton* results in back diffusion away from the meniscus opposite to the convective flow direction. During *Toff*, ions flow back toward the meniscus to compensate for the depleted ions. Additionally, water evaporates very fast from the meniscus, since the surface area to volume ratio (A/V) for small liquid meniscus is large. Fast evaporation of water from the meniscus increases the concentration of metal ions in the meniscus surface, which in turn results in additional convectional flow toward the meniscus area. One important advantage of evaporation in L-PED process is that the mass transport to the electrode is high, even in the absence of regular convection process used in bulk PED, such as stirring. This phenomenon results in a different range of process parameters compared to the bulk PED. Another consequence of high evaporation rate from the meniscus surface is higher ionic concentration at the meniscus edge, which cause non-uniform current density across the cathode surface. However, the controlled relative humidity and long OFF-time

period in the L-PED process allows the meniscus to achieve uniform ionic distribution across the cathode surface.

Energy dispersive X-ray spectroscopy (EDS)

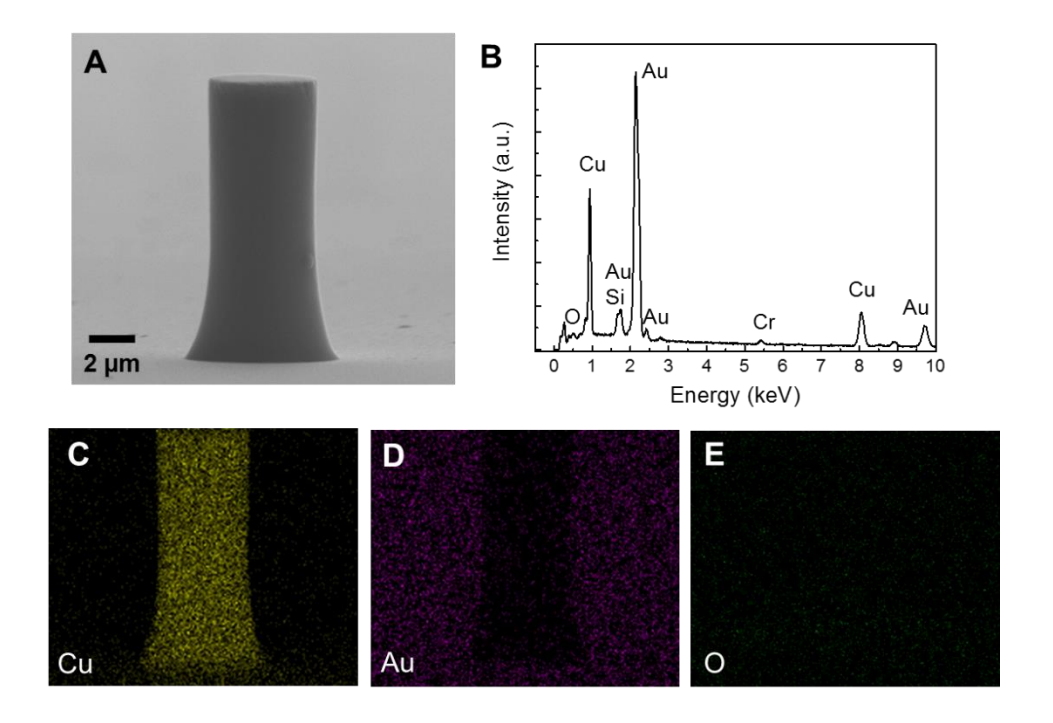


Figure S1. (A) Zoomed-in view of a single μ -pillar with a diameter of \sim 5.2 μ m from which the EDS spectra and map is shown in B-E. (B) The EDS spectra and (C)-(E) the EDS map acquired from the μ -pillar shown in B. No significant presence of impurities was observed in EDS data.

Effect of process parameters in L-PED

Table S1 The process parameters of the μ -pillars printed using the L-PED process.

Electrodeposition Mode	ON Time (s)	OFF Time (s)	Peak Current Density (A/cm²)	Average Current Density (mA/cm ²)		Current Efficiency (%)
L-PED	0.02	2	0.55	5.46	2	99
L-PED	0.02	4	2.28	11.37	5	94
L-PED	0.02	2	2.77	27.48	10	99
L-PED	0.02	4	6.98	34.73	12	94
L-PED	0.2	2	0.64	59.25	18	83
L-PED	0.02	2	7.34	72.68	24	90
L-PED	0.02	2	9.85	97.52	35	98

Effect of the process parameters in DC-ED

It is generally accepted that increasing the current density in electroplating of thin films promotes larger nucleation rate, which in turn results in grain refinement $^{[6]}$. Based on the Faraday's equation $^{[4]}$, the deposition rate of the metal in ED is proportional to the applied current density. We deposited μ -pillars with the same nozzle diameter, by varying the applied current to obtain different current densities, and hence difference deposition rates. We obtained deposition rates from \sim 7 nm/s to \sim 200 nm/s for current density of \sim 20 mA/cm² to \sim 550 mA/cm². The average CE (current efficiency) of the Cu deposition for the direct current electrodeposition (DC-ED, T_{OFF} = 0) was calculated to be 95 \pm 4 % (Figure S2).

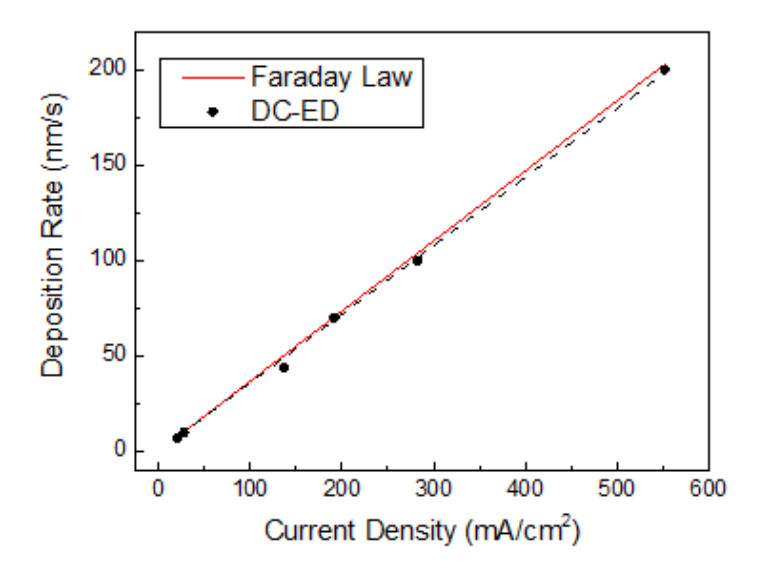


Figure S2. The Comparison of the obtained deposition rates of printed pillars by DC-ED process with the analytical growth rate calculated from the Faradays law. The obtained average current efficiency of DC-ED was calculated to be 95 ± 4 %.

Applying a constant voltage (DC-ED) during the printing process results in a nanocrystalline microstructure with uniformly scattered grains. μ-pillars with different parameters were printed using DC-ED to investigate the effect of the current density on the microstructure of the metal. We observed that by changing the current density, the average grain size of the printed Cu can be controlled (Figure S3), which is in agreement with the bulk electrodeposition process [7]. Specifically, it was found that in the printing process, the larger current density results in reduction of the average grain size in the printed metal (Table S2 and Figure S3).

Table S2 The process parameters of the μ -pillars printed using DC-ED technique.

Electrodeposition Mode	Current Density (mA/cm2)	Depostion Rate (nm/s)	Average Grain Size (nm)	Current Efficiency (%)
DC-ED	20	7	307 ± 47	94
DC-ED	28	10	263 ± 53	98
DC-ED	192	70	174 ± 52	99
DC-ED	283	100	121 ± 18	96
DC-ED	552	200	114 ± 14	99

Figure S3A-C shows the cross-section FIB ion-channeling contrast images of selected μ -pillars printed using current densities of 20 mA/cm², 192 mA/cm², and 283 mA/cm², corresponding to deposition rates of 7 nm/s, 70 nm/s, and 100 nm/s. Clearly, the average grain size reduces by increasing the current density and deposition rate. The average grain size was estimated using intercept procedure by counting the number of grains in the FIB cross-section image intercepted by sufficient number of straight lines widely separated. Quantitatively, the average grain size reduced from 307 \pm 47 nm to 121 \pm 18 nm for deposition rate of 7 nm/s to 100 nm/s.

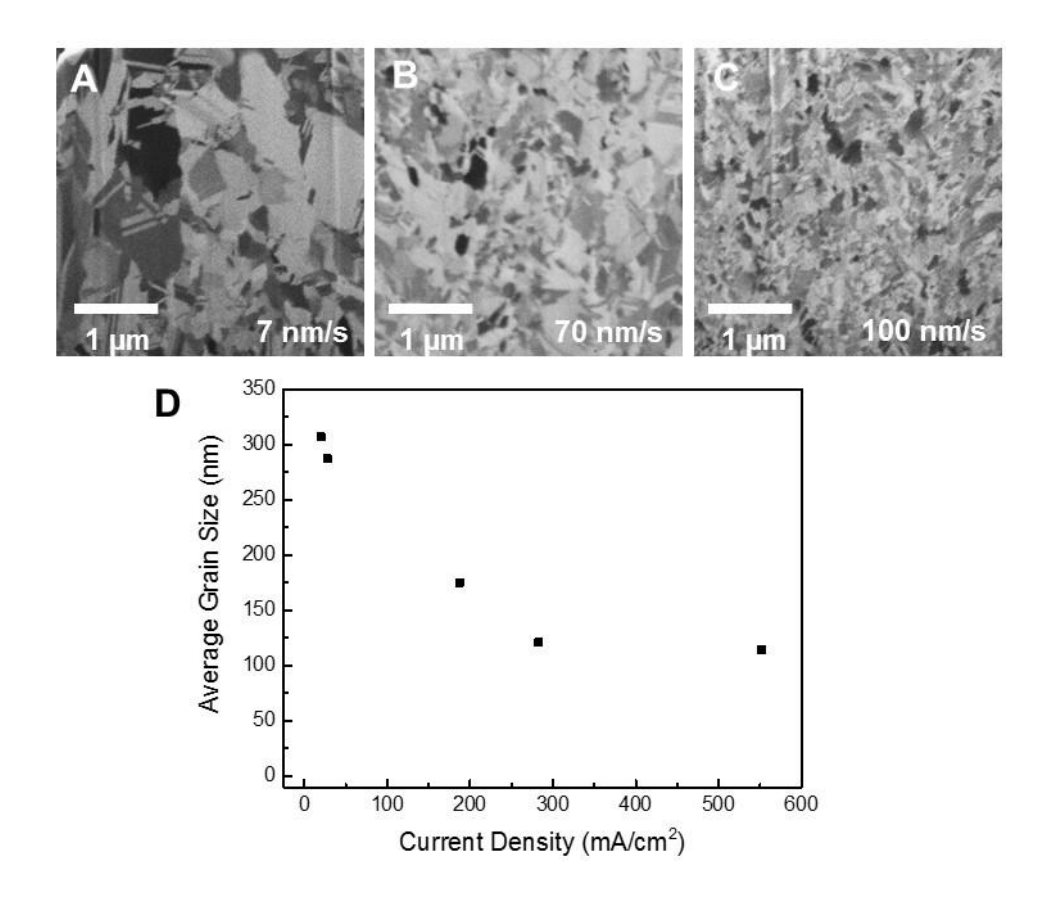


Figure S3. (A)-(C) The effect of the current density and deposition rate on the microstructure of Cu printed by DC-ED process. The cross-section FIB ion channeling contrast images of selected pillars show that increasing deposition current density causes grain refinement. The grain sizes of the pillars are (A) 307 ± 47 nm (B) 174 ± 52 nm (C) 121 ± 18 nm. (D) Average grain size vs. current density for the metal printed using the DC-ED process.

References

- [1] a) S. Daryadel, A. Behroozfar, S. R. Morsali, S. Moreno, M. Baniasadi, J. Bykova, R. A. Bernal, M. Minary-Jolandan, *Nano Letters* 2018, 18, 208; b) A. Behroozfar, S. Daryadel, S. R. Morsali, S. Moreno, M. Baniasadi, A. Bernal Rodrigo, M. Minary-Jolandan, *Advanced materials* 2017, 30, 1705107.
- [2] a) M. S. Chandrasekar, M. Pushpavanam, *Electrochimica Acta* 2008, 53, 3313; b) J. B. Marro, T. Darroudi, C. A. Okoro, Y. S. Obeng, K. C. Richardson, *Thin solid films* 2017, 621, 91; c) B. Z. Cui, K. Han, Y. Xin, D. R. Waryoba, A. L. Mbaruku, *Acta Materialia* 2007, 55, 4429; d) G.-T. Lui, D. Chen, J.-C. Kuo, *Journal of Physics D: Applied Physics* 2009, 42, 215410; e) Y. W. Lin, J. C. Kuo, K. T. Lui, D. Chen, *Materials Science Forum* 2010, 638-642, 2841.
- [3] H. Natter, R. Hempelmann, *The Journal of Physical Chemistry* **1996**, 100, 19525.

- [4] A. J. Bard, L. R. Faulkner, W. John, Sons, *Electrochemical methods : fundamentals and applications*, John Wiley & Sons, Hoboken **2007**.
- [5] a) S. Morsali, S. Daryadel, Z. Zhou, A. Behroozfar, M. Baniasadi, S. Moreno, D. Qian, M. Minary-Jolandan, *Journal of Applied Physics* 2017, 121, 214305; b) S. Morsali, S. Daryadel, Z. Zhou, A. Behroozfar, D. Qian, M. Minary-Jolandan, *Journal of Applied Physics* 2017, 121, 024903.
- [6] W. Dini Jack, D. Snyder Dexter, Modern Electroplating 2011.
- [7] H. Wang, P. Cheng, H. Wang, R. Liu, L. Sun, Q. Rao, Z. Wang, T. Gu, G. Ding, *Materials Characterization* **2015**, 109, 164.